Hyperspectral Image Restoration via Multi-mode and Double-weighted Tensor Nuclear Norm Minimization

Sheng Liu, Xiaozhen Xie, and Wenfeng Kong

***Abstract*—Tensor nuclear norm (TNN) induced by tensor singular value decomposition plays an important role in hyperspectral image (HSI) restoration tasks. In this letter, we first consider three inconspicuous but crucial phenomenons in TNN. In the Fourier transform domain of HSIs, different frequency components contain different information; different singular values of each frequency component also represent different information. The two physical phenomenons lie not only in the spectral dimension but also in the spatial dimensions. Then, to improve the capability and flexibility of TNN for HSI restoration, we propose a multi-mode and double-weighted TNN based on the above three crucial phenomenons. It can adaptively shrink the frequency components and singular values according to their physical meanings in all modes of HSIs. In the framework of the alternating direction method of multipliers, we design an effective alternating iterative strategy to optimize our proposed model. Restoration experiments on both synthetic and real HSI datasets demonstrate their superiority against related methods.**

***Index Terms*—Hyperspectral image, tensor nuclear norm, double weighting, frequency components, multi-mode.**

I. Introduction

HYPERSPECTRAL image (HSI) has been widely used in many fields [1, 2] due to its wealthy spatial and spectral information of a real scene. However, the observed HSIs are usually corrupted by different noises, e.g., Gaussian noise, impulse noise, deadlines, stripes and their mixtures. Therefore, HSI restoration, as a preprocessing step to remove mixed noise for various subsequent applications, is a valuable and active research topic.

HSIs can be treated as 3-order tensors. Its low-rankness is a critical property for HSI restoration tasks. Due to the nonunique definitions of the tensor rank, different tensor decompositions and their corresponding tensor ranks are proposed, such as the Tucker decomposition [3, 4], PARAFAC decomposition [5, 6], and tensor singular value decomposition (t-SVD) [7–9], to exploit the low-rankness of HSIs.

Among them, the tensor tubal rank induced by t-SVD can characterize the low-rank structure of a tensor very well [10]. Its convex relaxation is the tensor nuclear norm (TNN) [11]. TNN is effective to keep the intrinsic structure of tensors; t-SVD can be calculated easily in the Fourier domain and TNN minimization problem can be efficiently solved by convex optimization algorithms. Hence, TNN has attracted extensive attention for HSI restoration problems in recent years [8, 12, 13]. However, during the definition of TNN, there are three kinds of prior knowledge that are underutilized for further exploiting the low-rankness in HSIs. Firstly, in the Fourier transform domain of HSIs, the low-frequency slices carry the profile information of HSIs, while the high-frequency slices mainly carry the detail and noise information of HSIs. Secondly, in each frequency slices, bigger singular values mainly contain information on clean data and smaller singular values mainly contain information on noise. Thirdly, low-rankness not only exists in the spectral dimension but also lies in the spatial dimensions [3]. The classical TNN only takes the Fourier transform to connect the spatial dimensions with the spectral dimension and lacks flexibility for handling different correlations along with different modes of HSIs [8].

In this letter, to take full advantage of the above prior knowledge and improve the capability and flexibility of TNN, we propose a multi-mode and double-weighted TNN (MDWTNN) for HSI restoration tasks. The merits of our model are four-fold. First, according to information types in different frequency slices in the Fourier transform domain, we adaptively assign bigger weights to slices that mainly contain noise information and smaller weights to slices that mainly contain profile information, which can depress noise more and simultaneously preserve the profile information of clean HSIs better. Second, in each frequency slice, we use the partial sum of singular values (PSSV) to only shrink small singular values, which can better protect the clean data information contained in big singular values. Third, we apply the double-weighted TNN in all modes of HSIs, which can achieve a more flexible and accurate characterization of HSI low-rankness. Finally, we develop an alternating direction method of multiplier (ADMM) based algorithm to efficiently solve the proposed model, and obtain the best restoration performance both on the synthetic and real HSI dataset in comparison to all competing HSI restoration methods.

II. Preliminaries

A. Notations

In this letter, matrix and tensor are denoted as bold uppercase letter $\mathbf{X}$ and calligraphic letter $\mathcal{X}$, respectively. For a 3rd-order tensor $\mathcal{X} \in \mathbb{R}^{n_1 \times n_2 \times n_3}$, its (i, j, k)-th component is represented as $\mathcal{X}(i, j, k)$. For $\mathcal{X}$, $\mathcal{Y} \in \mathbb{R}^{n_1 \times n_2 \times n_3}$, their inner

This work was supported by the Undergraduate Innovation and Entrepreneurship Project of China under Grant S202010712032, S202010712294 and X202010712196. (Corresponding author: Xiaozhen Xie.)

Sheng Liu, Xiaozhen Xie, and Wenfeng Kong are with College of Science, Northwest A&F University, Yangling 712100, China (e-mail: liusheng16@163.com; e-mail: xiexzh@nwafu.edu.cn; e-mail: kksama@nwafu.edu.cn).

product is defined as $< \mathcal{X}, \mathcal{Y} >= \sum_{i=1}^{n_1} \sum_{j=1}^{n_2} \sum_{k=1}^{n_3} x_{ijk} y_{ijk}$. Then the Frobenius norm of a tensor $\mathcal{X}$ is defined as $\|\mathcal{X}\|_F = \sqrt{< \mathcal{X}, \mathcal{X} >}$. The k-th frontal slice of $\mathcal{X}$ is denoted as $\mathbf{X}^{(k)} = \mathcal{X}(:,:,k)$. The fast Fourier transform along the third mode of $\mathcal{X}$ is represented as $\bar{\mathcal{X}} = \texttt{fft}(\mathcal{X}, [], 3)$ and its inverse operation is $\mathcal{X} = \texttt{ifft}(\bar{\mathcal{X}}, [], 3)$. The mode-$p$ permutation of $\mathcal{X}$ is defined as $\mathcal{X}_p = \texttt{permute}(\mathcal{X}, p)$, $p = 1, 2, 3$, where the m-th mode-3 slice of $\mathcal{X}_p$ is the m-th mode-p slice of $\mathcal{X}$, i.e., $\mathcal{X}(i,j,k) = \mathcal{X}_1(j,k,i) = \mathcal{X}_2(k,i,j) = \mathcal{X}_3(i,j,k)$. Also, its inverse operation is $\mathcal{X} = \texttt{ipermute}(\mathcal{X}_p, p)$.

B. Problem Formulation

An ideal HSI can be viewed as a 3rd-order tensor $\mathcal{X} \in \mathbb{R}^{n_1 \times n_2 \times n_3}$ and usually is assumed to be low-rank. Corrupted by mixed noise, its observed version can be modeled as

$$\mathcal{Y} = \mathcal{X} + \mathcal{S} + \mathcal{N}, \tag{1}$$

where $\mathcal{Y}, \mathcal{S}, \mathcal{N} \in \mathbb{R}^{n_1 \times n_2 \times n_3}$; $\mathcal{S}$ denotes the sparse noise; $\mathcal{N}$ denotes the Gaussian white noise.

HSI restoration aims to recover the ideal HSI $\mathcal{X}$ from the observed HSI $\mathcal{Y}$ in (1). Under the framework of regularization theory, it can briefly be formulated as

$$\begin{aligned} \arg \min_{\mathcal{X},\mathcal{S},\mathcal{N}} & \texttt{Rank}(\mathcal{X}) + \lambda \|\mathcal{S}\|_1 + \tau \|\mathcal{N}\|_F^2, \\ s.t. & \mathcal{Y} = \mathcal{X} + \mathcal{S} + \mathcal{N}, \end{aligned} \tag{2}$$

where $\|\cdot\|_1$ is L_1 norm to detect the sparse noise; $\|\cdot\|_F$ describes the Gaussian noise; $\texttt{Rank}(\cdot)$ represents the rank of unknown ideal HSI; λ and τ are non-negative parameters.

In model (2), regularization term $\texttt{Rank}$ is approximated by different relaxations. As mentioned above, TNN is widely used convex relaxation, which can be defined as

$$\|\mathcal{X}\|_* := \frac{1}{n_3} \sum_{k=1}^{n_3} \|\bar{\mathbf{X}}^{(k)}\|_*. \tag{3}$$

III. The Proposed Weighted TNN

A. Frequency-Weighted TNN

In (3), we notice that one frontal slice of $\bar{\mathcal{X}}$ corresponds to one frequency component of $\mathcal{X}$. Specifically, for $\mathcal{X}$, its profile information is contained in the low-frequency frontal slices, while its detailed information is contained in the high-frequency ones. When $\mathcal{X}$ is distorted by outliers, the effects on high-frequency frontal slices are more severe. However, different frequency slices of $\bar{\mathcal{X}}$ have the same impact on TNN in (3), which is obviously inconsistent with the physics meaning of frequency components. Therefore, we improve TNN in (3) by assigning different weights for different frequency slices, and propose the frequency-weighted TNN as follows:

$$\|\mathcal{X}\|_{w*} := \sum_{k=1}^{n_3} w_k(\bar{\mathbf{X}}^{(k)}) \|\bar{\mathbf{X}}^{(k)}\|_*, \tag{4}$$

where $w_k(\bar{\mathbf{X}}^{(k)})$ is the k-th weight parameter. For HSI restoration problems, the lower the frequencies are, the less the corresponding frequency slices should be punished. By amounts of data simulations, the weights w_k approximatively consist with the frequencies and are inversely proportionate to $\|\bar{\mathbf{X}}^{(k)}\|_F$. We let

$$w_k(\bar{\mathbf{X}}^{(k)}) = \frac{c_1}{\log(\|\bar{\mathbf{X}}^{(k)}\|_F^2) + \varepsilon} + c_2, \tag{5}$$

where $\varepsilon = 10^{-10}$ is to avoid dividing by zero; c_1 and c_2 are two parameters.

B. Double-Weighted TNN

For $\bar{\mathbf{X}}^{(k)}$ in (3), the matrix nuclear norm is used as the tightest convex surrogate for rank. However, it has limitation in the accuracy of approximation due to its convexity. Recently, a series of improvement methods are proposed for better approximation [14–17]. To differently treat singular values of $\bar{\mathbf{X}}^{(k)}$, we choose partial sum of singular values (PSSV) to only punish the smaller singular values which mainly contain the noise information of HSIs. Then, a double-weighted TNN is proposed by replacing the matrix nuclear norm in (4) with the PSSV of $\bar{\mathbf{X}}^{(k)}$, which is defined as

$$\|\mathcal{X}\|_{dw*} := \frac{1}{n_3} \sum_{k=1}^{n_3} w_k(\bar{\mathbf{X}}^{(k)}) \|\bar{\mathbf{X}}^{(k)}\|_{\text{PSSV}}, \tag{6}$$

where $\|\bar{\mathbf{X}}^{(k)}\|_{\text{PSSV}} = \sum_{r=R+1}^{\min\{n_1,n_2\}} \sigma_r(\bar{\mathbf{X}}^{(k)})$; $\sigma_r(\bar{\mathbf{X}}^{(k)})$ is the r-th biggest singular value of matrix $\bar{\mathbf{X}}^{(k)}$; R is a parameter indicating the number of main singular values. The double-weighted TNN minimization problem can be solved by following theorem.

Theorem 1. Assuming that $\tau > 0$, $\mathcal{X}, \mathcal{Y} \in \mathbb{R}^{n_1 \times n_2 \times n_3}$, for the minimization problem

$$\mathcal{X}^* = \arg\min_{\mathcal{X}} \tau \|\mathcal{X}\|_{dw*} + \frac{1}{2} \|\mathcal{X} - \mathcal{Y}\|_F^2, \tag{7}$$

its solution is

$$\mathcal{X}^* = \mathcal{DW}^{w,R,\tau}(\mathcal{Y}) = \texttt{ifft}(\bar{\mathcal{U}} \cdot \bar{\mathcal{S}}_{dw*} \cdot \bar{\mathcal{V}}^T, [], 3), \tag{8}$$

where $\bar{\mathcal{Y}} = \bar{\mathcal{U}} \cdot \bar{\mathcal{S}} \cdot \bar{\mathcal{V}}^T$; $\bar{\mathcal{S}}_{dw*}(r,r,k) = \max(\bar{\mathcal{S}}(r,r,k) - \tau w_r w_k, 0)$; $w_r = \begin{cases} 0, & r \le R \\ 1, & r > R \end{cases}$; $w_k = \frac{c_1}{\log(\|\bar{\mathbf{X}}^{(k)}\|_F^2 + \varepsilon)} + c_2$.

C. Multi-mode and Double-Weighted TNN

TNN in (3) only approximates the correlations connected by mode-3 Fourier transform in the spatial dimensions with the spectral dimension. It lacks of flexibility for describing low-rankness in all modes of HSIs. To connect the p-th mode with other two modes, we can define the double-weighted TNN for each mode-p permutation of HSIs, i.e., $\|\mathcal{X}_p\|_{dw*}, p = 1, 2, 3$. As $\|\mathcal{X}_p\|_{dw*}$ are different according to different modes, we use the weighted average of double-weighted TNNs along all modes to approximate the tensor rank of HSIs. Finally, the multi-mode and double-weighted TNN (MDWTNN) is proposed as follows:

$$\|\mathcal{X}\|_{mdw*} := \sum_{p=1}^{3} \alpha_p \|\mathcal{X}_p\|_{dw*} = \sum_{p=1}^{3} \sum_{k=1}^{n_p} \alpha_p w_k^p \|\bar{\mathbf{X}}_p^{(k)}\|_{\text{PSSV}}, \tag{9}$$

where $\bar{\mathcal{X}}_p = \texttt{fft}(\mathcal{X}_p, [], 3)$; $\bar{\mathbf{X}}_p^{(k)}$ is the k-th frontal slice of $\bar{\mathcal{X}}_p$ and its assigned weight is w_k^p; $\alpha_p > 0$ and $\sum_{p=1}^{3} \alpha_p = 1$.

IV. HSI Restoration via MDWTNN Minimization

MDWTNN in (9) takes full advantage of physical meanings in frequency components, singular values, and modes of HSIs, which can provide a better approximation to the tensor rank. Then we use MDWTNN to replace the regularization term `Rank` in (2) and propose the HSI restoration model as follows:

$$\begin{aligned} \arg\min_{\mathcal{X},\mathcal{S},\mathcal{N}} \quad & \|\mathcal{X}\|_{mdw*} + \lambda\|\mathcal{S}\|_1 + \tau\|\mathcal{N}\|_F^2, \\ s.t. \quad & \mathcal{Y} = \mathcal{X} + \mathcal{S} + \mathcal{N}. \end{aligned} \tag{10}$$

Introducing auxiliary variables, model (10) is equivalent to

$$\begin{aligned} \arg\min_{\mathcal{X},\mathcal{S},\mathcal{N}} & \sum_{p=1}^{3} \alpha_p \|\mathcal{Z}_p\|_{dw*} + \lambda\|\mathcal{S}\|_1 + \tau\|\mathcal{N}\|_F^2, \\ s.t.\ & \mathcal{Y} = \mathcal{X} + \mathcal{S} + \mathcal{N},\ \mathcal{Z}_p = \mathcal{X}_p,\ p = 1,2,3. \end{aligned} \tag{11}$$

By augmented Lagrangian multiplier method, the Lagrangian function of model (11) can be written as

$$\begin{aligned} & L_{\mu_p,\beta}(\mathcal{X},\mathcal{Z}_p,\mathcal{N},\mathcal{S},\Gamma_p,\Lambda) = \lambda\|\mathcal{S}\|_1 + \tau\|\mathcal{N}\|_F^2 \\ & + < \mathcal{Y} - (\mathcal{X}+\mathcal{S}+\mathcal{N}), \Lambda > + \tfrac{\beta}{2}\|\mathcal{Y} - (\mathcal{X}+\mathcal{S}+\mathcal{N})\|_F^2, \\ & + \sum_{p=1}^{3} \Big\{ \alpha_p\|\mathcal{X}_p\|_{dw*} + < \mathcal{X}_p - \mathcal{Z}_p, \Gamma_p > + \frac{\mu_p}{2}\|\mathcal{X}_p - \mathcal{Z}_p\|_F^2 \Big\}, \end{aligned}$$

where Λ and Γ_p are the Lagrangian multipliers; β and μ_p are the Lagrange penalty parameters. Its minimization problem can be efficiently solved in the framework of ADMM [18]. At the $(n+1)$-th iteration, each variable in the Lagrangian function can be updated by solving its corresponding subproblem respectively when other variables are fixed at the n-th iteration.

For $\mathcal{Z}_p$, $p = 1,2,3$, their corresponding subproblems can be written as

$$\arg\min_{\mathcal{Z}_p} \alpha_p\|\mathcal{Z}_p\|_{dw*} + \frac{\mu_p}{2}\left\|\mathcal{Z}_p - \left(\mathcal{X}_p^n + \frac{\Gamma_p^n}{\mu_p}\right)\right\|_F^2. \tag{12}$$

The closed-form solution of (12) obtained from theorem 1 are as follows:

$$\mathcal{Z}_p^{n+1} = \mathcal{DW}^{w(\mathcal{X}_p^n),R,\frac{\alpha_p}{\mu_p}}\left(\mathcal{X}_p^n + \frac{\Gamma_p^n}{\mu_p}\right). \tag{13}$$

For $\mathcal{X}$, its corresponding subproblem can be written as

$$\begin{aligned} \mathcal{X}^{n+1} = & \arg\min_{\mathcal{X}} \sum_{p=1}^{3} \frac{\mu_p}{2}\|\mathcal{X} - \mathcal{Z}_p^{n+1} + \frac{\Gamma_p^n}{\mu_p}\|_F^2 \\ & + \frac{\beta}{2}\|\mathcal{Y} - (\mathcal{X} + \mathcal{S}^n + \mathcal{N}^n) + \frac{\Lambda^n}{\beta}\|_F^2. \end{aligned} \tag{14}$$

It has the closed-form solution as follows:

$$\mathcal{X}^{n+1} = \frac{\sum_{p=1}^{3}\mu_p\left(\mathcal{Z}_p^{n+1} - \frac{\Gamma_p^n}{\mu_p}\right) + \beta\left(\mathcal{Y} - \mathcal{S}^n - \mathcal{N}^n + \frac{\Lambda^n}{\beta}\right)}{1+\beta}. \tag{15}$$

For $\mathcal{S}$, its corresponding subproblem can be written as

$$\arg\min_{\mathcal{S}} \lambda\|\mathcal{S}\|_1 + \frac{\beta}{2}\|\mathcal{Y} - \left(\mathcal{X}^{n+1} + \mathcal{S} + \mathcal{N}^n\right) + \frac{\Lambda^n}{\beta}\|_F^2. \tag{16}$$

It can be solved by the soft-thresholding operator [19] as:

$$\mathcal{S}^{n+1} = \texttt{shrink}\left(\mathcal{Y} - \mathcal{X}^{n+1} - \mathcal{N}^{n+1} + \tfrac{\Lambda^n}{\beta}, \tfrac{\lambda}{\beta}\right). \tag{17}$$

For $\mathcal{N}$, its corresponding subproblem can be written as

$$\arg\min_{\mathcal{N}} \tau\|\mathcal{N}\|_F^2 + \frac{\beta}{2}\|\mathcal{Y} - \left(\mathcal{X}^{n+1} + \mathcal{S}^{n+1} + \mathcal{N}\right) + \frac{\Lambda^n}{\beta}\|_F^2. \tag{18}$$

It has the closed-form solution as follows :

$$\mathcal{N}^{n+1} = \frac{\beta\left(\mathcal{Y} - \mathcal{X}^{n+1} - \mathcal{S}^n + \frac{\Lambda^n}{\beta}\right)}{2\tau+\beta}. \tag{19}$$

For multipliers Γ_p and Λ, they can be updated as follows:

$$\begin{cases} \Gamma_p^{n+1} = \Gamma_p^n + \mu_p\left(\mathcal{Z}_p^{n+1} - \mathcal{X}^{n+1}\right), p = 1,2,3 \\ \Lambda^{n+1} = \Lambda^n + \beta\left(\mathcal{Y} - \mathcal{X}^{n+1} - \mathcal{S}^{n+1} - \mathcal{N}^{n+1}\right). \end{cases} \tag{20}$$

The proposed algorithm for our HSI restoration model is summarized in Algorithm 1.

Algorithm 1 HSI Restoration via the MDWTNN minimization

Input: The observed tensor $\mathcal{Y}$; weight parameters c_1, c_2, R; regularization parameters λ, τ; and stopping criterion ϵ.

Output: Denoised image $\mathcal{X}$.

1: Initialize: $\mathcal{Y}$=$\mathcal{X}$=$\mathcal{S}$=$\mathcal{N}$=$\mathcal{Z}_p$; $\Gamma_p = \Lambda = 0$; μ_p=β=10^{-3}; $p = 1,2,3$; $\mu_{max} = 10^{10}$; $\rho = 1.2$ and $n = 0$.
2: Repeat until convergence:
3. Update $\mathcal{X}, \mathcal{S}, \mathcal{N}, \mathcal{Z}_p, \Lambda$, β, μ_p, w_k, Γ_p via
  step 1: Update $\mathcal{Z}_p$ by (13)
  step 2: Update $\mathcal{X}$ by (15)
  step 3: Update $\mathcal{S}$ by (17)
  step 4: Update $\mathcal{N}$ by (19)
  step 5: Update Γ_p, Λ by (20)
  step 6: Update $\mu_p = \rho\mu_p$, $\beta = \rho\beta$, w_k by (5)
4: Check the convergence condition.

V. Experiments

To verify the effectiveness of our MDWTNN based HSI restoration model, various experiments are performed on two challenging simulated datasets and a real HSI datasets. From the Washington DC Mall dataset[1], we choose a sub-blocks with a size of $256 \times 256 \times 191$ as a simulation dataset. From the Pavia City Center dataset[2], we choose a sub-blocks with a size of $200 \times 200 \times 80$ as a simulation dataset. From the Indian Pines dataset[3], we choose a sub-blocks with a size of $145 \times 145 \times 220$ as a real dataset. For comparison, four state-of-the-art HSI denoising methodes are employed as the benchmark in the experiments, i.e., BM4D [20], LRMR [21], LRTDTV [3] and 3DTNN [8]. Since the BM4D method is only suitable to remove Gaussian noise, we implement it on HSIs which are preprocessed by the RPCA restoration method [7].

In the simulation experiments, the hybrid of white Gaussian and impulse noises with 5 different intensity levels are added to the simulation dataset band by band. Let G and P denote the variance of Gaussian white noise and percentage of impulse noise, respectively. In noise case 1-3, the same intensity noise is added to all the bands. In noise case 1, G=0.1 and P=0.2; In noise case 2, G=0.2 and P=0.2; In noise case 3, G=0.1 and P=0.4; In noise case 4 and 5, the noise intensities are different for different bands. In noise case 4, G is randomly selected from 0.1 to 0.2 and P=0.2; In noise case 5, G=0.1 and P is randomly selected from 0.2 to 0.4.

For quantitatively evaluating the restoration results of all the test methods, the CPU times and the means of PSNR [22],

[1] http://lesun.weebly.com/hyperspectral-data-set.html
[2] http://www.ehu.eus/ccwintco/index.php/
[3] https://engineering.purdue.edu/biehl/MultiSpec/hyperspectral

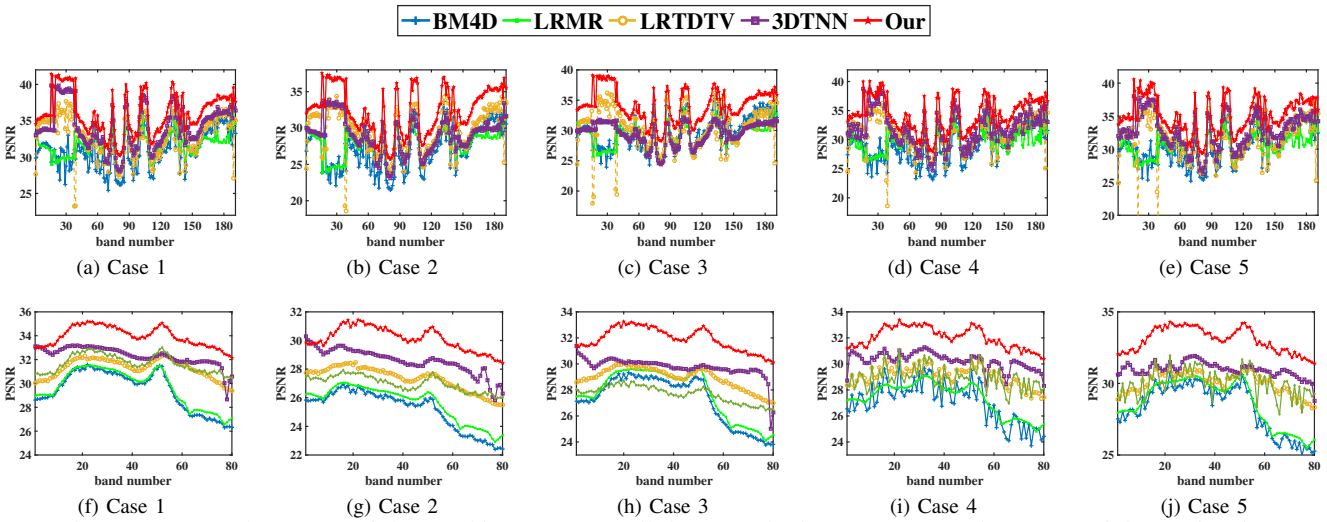

(a) Case 1 (b) Case 2 (c) Case 3 (d) Case 4 (e) Case 5

(f) Case 1 (g) Case 2 (h) Case 3 (i) Case 4 (j) Case 5

Fig. 1: The top row are the PSNR of the Washington DC Mall dataset. The bottom row are the PSNR of the Pavia City Center dataset. From left column to right column, PSNR of each band in all restoration results under noise case 1-5.

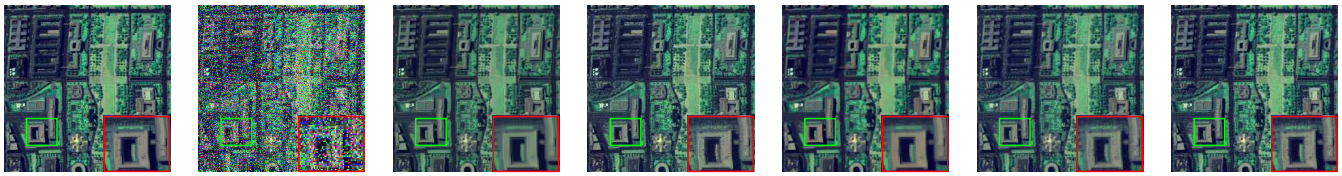

(a) Original image (b) Noise image (c) BM4D(27.75dB) (d) LRMR(29.38dB) (e) LRTDTV (28.58dB) (f) 3DTNN(29.89dB) (g) Our(32.09dB)

Fig. 2: The restoration results for the Washington DC Mall dataset under noise case 5. Pseudocolor image with bands (115, 80, 58).

(a) Original image (b) Noise image (c) BM4D(24.53dB) (d) LRMR(27.84dB) (e) LRTDTV (27.13dB) (f) 3DTNN(27.55dB) (g) Our(28.08dB)

Fig. 3: The restoration results for the Pavia City Center dataset under noise case 1. Pseudocolor image with bands (78, 58, 14).

(a) Noise image (b) LRTA (c) BM4D (d) LRMR (e) LRTDTV (f) 3DTNN (g) Our

Fig. 4: The 150-th band of all restoration results for the real dataset.

SSIM [23] and SAM [24] in each band, i.e., MPSNR, MSSIM and MSAM, are listed in Table I. Also, the PSNR of each band in all restoration results on both simulated datasets are presented in Fig. 1. It is clear that our proposed model enjoys a superior performance over the other popular approaches. Although the CPU times of our model are not the shortest, one can update $\mathcal{Z}_p$ by (13) in parallel to further shorten the CPU times of our model. For visual evaluation in Fig. 2 and Fig. 3 , We show the restoration results of the Washington DC Mall dataset in Case 5 and the Pavia City Center dataset in Case 1 respectively. In Fig. 4, we list the 150-th in all restoration results of the real dataset. It can be seen that the image restored by our model maintains the best structure and texture information.

VI. Conclusion

In this letter, we propose a multi-mode and double-weighted TNN for HSI restoration tasks. The proposed TNN can efficiently characterize the physical meanings of the frequency components, singular values, and orientations ignored by the standard TNN. And the weight parameters also can be obtained adaptively. They powerfully improve capability and

TABLE I: Quantitative comparison and time of all competing methods under different levels of noises on simulate dataset.

Dataset	Noise case	Index	Noise	BM4D	LRMR	LRTDTV	3DTNN	Our
Washington DC Mall	Case1	PSNR	11.068	31.014	31.567	32.800	34.270	**36.095**
		SSIM	0.085	0.893	0.867	0.896	0.936	**0.950**
		MSAM	43.139	4.576	5.042	4.327	3.481	**2.937**
		TIME	-	547.005	378.898	538.160	270.211	334.656
	Case2	PSNR	10.216	27.192	27.642	29.489	29.055	**32.525**
		SSIM	0.061	0.791	0.743	0.807	0.801	**0.894**
		MSAM	45.297	6.830	7.859	6.382	6.726	**4.393**
		TIME	-	529.243	395.461	584.461	309.977	378.728
	Case3	PSNR	8.305	29.691	29.183	30.270	29.572	**34.185**
		SSIM	0.037	0.866	0.798	0.844	0.784	**0.928**
		MSAM	50.092	5.264	6.579	6.182	6.542	**3.604**
		TIME	-	528.440	394.272	582.318	316.547	375.719
	Case4	PSNR	10.648	28.970	29.518	31.073	31.852	**34.379**
		SSIM	0.073	0.848	0.810	0.859	0.887	**0.930**
		MSAM	44.265	5.695	6.439	5.468	4.873	**3.579**
		TIME	-	541.960	396.478	537.374	273.466	340.113
	Case5	PSNR	9.669	30.419	30.412	31.560	32.783	**35.180**
		SSIM	0.060	0.883	0.836	0.874	0.902	**0.942**
		MSAM	47.270	4.865	5.761	5.405	4.311	**3.220**
		TIME	-	546.378	397.474	541.124	277.123	340.162
Pavia City Center	Case1	MPSNR	11.122	29.701	31.259	32.297	31.696	**33.951**
		MSSIM	0.105	0.920	0.905	0.914	0.924	**0.942**
		MSAM	45.712	5.84	6.824	4.93	4.844	**4.426**
		time	-	112.235	113.723	131.91	54.461	72.224
	Case2	MPSNR	10.265	25.619	27.321	28.605	27.009	**30.124**
		MSSIM	0.074	0.835	0.791	0.821	0.799	**0.879**
		MSAM	46.978	7.170	8.385	6.685	6.923	**5.666**
		time	-	113.246	113.115	129.155	56.610	71.322
	Case3	MPSNR	8.384	27.745	28.937	29.741	27.696	**31.924**
		MSSIM	0.043	0.892	0.848	0.873	0.790	**0.916**
		MSAM	48.580	6.745	7.74	6.007	9.875	**5.095**
		time	-	115.908	116.961	127.981	54.448	71.435
	Case4	MPSNR	10.659	27.361	29.094	30.251	28.934	**32.041**
		MSSIM	0.088	0.877	0.853	0.870	0.860	**0.915**
		MSAM	46.457	6.6	7.796	5.877	6.389	**5.048**
		time	-	115.684	133.241	129.088	51.669	68.251
	Case5	MPSNR	9.565	28.674	30.044	30.977	30.055	**33.038**
		MSSIM	0.070	0.907	0.878	0.893	0.879	**0.932**
		MSAM	47.885	6.293	7.333	5.493	6.795	**4.682**
		time	-	133.811	81.989	120.418	61.742	77.520

flexibility for describing low-rankness in HSIs. The experiments conducted with both simulate and real HSI datasets show that our MDWTNN based HSI restoration model is a competitive method to remove the hybrid noise. Besides, our proposed MDWTNN regularization term can also be applied to other low-rankness based tasks, i.e., hyperspectral imagery classification, tensor completion, MRI reconstruction.

REFERENCES

[1] A. F. Goetz, "Three decades of hyperspectral remote sensing of the earth: A personal view," *Remote Sensing of Environment*, vol. 113, pp. S5–S16, 2009.

[2] J. M. Bioucas-Dias, A. Plaza, G. Camps-Valls, P. Scheunders, N. Nasrabadi, and J. Chanussot, "Hyperspectral remote sensing data analysis and future challenges," *IEEE Geoscience and Remote Sensing Magazine*, vol. 1, no. 2, pp. 6–36, 2013.

[3] Y. Wang, J. Peng, Q. Zhao, Y. Leung, X.-L. Zhao, and D. Meng, "Hyperspectral image restoration via total variation regularized low-rank tensor decomposition," *IEEE Journal of Selected Topics in Applied Earth Observations and Remote Sensing*, vol. 11, no. 4, pp. 1227–1243, 2017.

[4] D. Letexier and S. Bourennane, "Noise removal from hyperspectral images by multidimensional filtering," *IEEE Transactions on Geoscience and Remote Sensing*, vol. 46, no. 7, pp. 2061–2069, 2008.

[5] X. Liu, S. Bourennane, and C. Fossati, "Denoising of hyperspectral images using the parafac model and statistical performance analysis," *IEEE Transactions on Geoscience and Remote Sensing*, vol. 50, no. 10, pp. 3717–3724, 2012.

[6] X. Huang, S. Xu, C. Zhang, and J. Zhang, "Robust cp tensor factorization with skew noise," *IEEE Signal Processing Letters*, vol. 27, pp. 785–789, 2020.

[7] C. Lu, J. Feng, Y. Chen, W. Liu, Z. Lin, and S. Yan, "Tensor robust principal component analysis with a new tensor nuclear norm," *IEEE Transactions on Pattern Analysis and Machine Intelligence*, vol. 42, no. 4, pp. 925–938, 2019.

[8] Y.-B. Zheng, T.-Z. Huang, X.-L. Zhao, T.-X. Jiang, T.-H. Ma, and T.-Y. Ji, "Mixed noise removal in hyperspectral image via low-fibered-rank regularization," *IEEE Transactions on Geoscience and Remote Sensing*, vol. 58, no. 1, pp. 734–749, 2019.

[9] T.-X. Jiang, T.-Z. Huang, X.-L. Zhao, and L.-J. Deng, "Multi-dimensional imaging data recovery via minimizing the partial sum of tubal nuclear norm," *Journal of Computational and Applied Mathematics*, vol. 372, p. 112680, 2020.

[10] Z. Zhang, G. Ely, S. Aeron, N. Hao, and M. Kilmer, "Novel methods for multilinear data completion and de-noising based on tensor-svd," in *Proceedings of the IEEE Conference on Computer Vision and Pattern Recognition*, 2014, pp. 3842–3849.

[11] M. E. Kilmer, K. Braman, N. Hao, and R. C. Hoover, "Third-order tensors as operators on matrices: A theoretical and computational framework with applications in imaging," *SIAM Journal on Matrix Analysis and Applications*, vol. 34, no. 1, pp. 148–172, 2013.

[12] H. Zeng, X. Xie, H. Cui, H. Yin, and J. Ning, "Hyperspectral image restoration via global l_{1-2} spatial-spectral total variation regularized local low-rank tensor recovery," *IEEE Transactions on Geoscience and Remote Sensing*, 2020.

[13] H. Zeng, X. Xie, and J. Ning, "Hyperspectral image denoising via global spatial-spectral total variation regularized nonconvex local low-rank tensor approximation," *Signal Processing*, vol. 178, p. 107805, 2021.

[14] T.-H. Oh, Y.-W. Tai, J.-C. Bazin, H. Kim, and I. S. Kweon, "Partial sum minimization of singular values in robust pca: Algorithm and applications," *IEEE transactions on Pattern Analysis and Machine Intelligence*, vol. 38, no. 4, pp. 744–758, 2015.

[15] S. Gu, L. Zhang, W. Zuo, and X. Feng, "Weighted nuclear norm minimization with application to image denoising," in *Proceedings of the IEEE conference on computer vision and pattern recognition*, 2014, pp. 2862–2869.

[16] Y. Chen, Y. Guo, Y. Wang, D. Wang, C. Peng, and G. He, "Denoising of hyperspectral images using nonconvex low rank matrix approximation," *IEEE Transactions on Geoscience and Remote Sensing*, vol. 55, no. 9, pp. 5366–5380, 2017.

[17] T.-Y. Ji, T.-Z. Huang, X.-L. Zhao, T.-H. Ma, and L.-J. Deng, "A non-convex tensor rank approximation for tensor completion," *Applied Mathematical Modelling*, vol. 48, pp. 410–422, 2017.

[18] S. Boyd, N. Parikh, and E. Chu, *Distributed optimization and statistical learning via the alternating direction method of multipliers*. Now Publishers Inc, 2011.

[19] Z. Lin, M. Chen, and Y. Ma, "The augmented lagrange multiplier method for exact recovery of corrupted low-rank matrices," *arXiv preprint arXiv:1009.5055*, 2010.

[20] M. Maggioni and A. Foi, "Nonlocal transform-domain denoising of volumetric data with groupwise adaptive variance estimation," in *Computational Imaging X*, vol. 8296. International Society for Optics and Photonics, 2012, p. 82960O.

[21] H. Zhang, W. He, L. Zhang, H. Shen, and Q. Yuan, "Hyperspectral image restoration using low-rank matrix recovery," *IEEE Transactions on Geoscience and Remote Sensing*, vol. 52, no. 8, pp. 4729–4743, 2013.

[22] Q. Huynh-Thu and M. Ghanbari, "Scope of validity of psnr in image/video quality assessment," *Electronics Letters*, vol. 44, no. 13, pp. 800–801, 2008.

[23] Z. Wang, A. C. Bovik, H. R. Sheikh, E. P. Simoncelli *et al.*, "Image quality assessment: from error visibility to structural similarity," *IEEE Transactions on Image Processing*, vol. 13, no. 4, pp. 600–612, 2004.

[24] F. Kruse, A. Lefkoff, and J. Dietz, "Expert system-based mineral mapping in northern death valley, california/nevada, using the airborne visible/infrared imaging spectrometer (aviris)," *Remote Sensing of Environment*, vol. 44, no. 2-3, pp. 309–336, 1993.